A Runge-Kutta discontinuous Galerkin scheme for the ideal Magnetohydrodynamical model

Praveen Chandrashekar, Juan Pablo Gallego-Valencia and Christian Klingenberg

Abstract A numerical scheme for solving the system of ideal Magneto- Hydrodynamical (MHD) model, using an explicit high order Runge-Kutta discontinuous Galerkin method (RKDG) is proposed. An entropy stable numerical flux introduced in the context of Finite Volume (FV) method in [4] is used in the RKDG scheme. To illustrate the usefulness of the implementation, some specific test cases for the ideal magneto-hydrodynamical model (MHD equations) are shown.

1 Introduction

As a part of the EXAMAG project of the SPPEXA priority project funded by the DFG, a Runge-Kutta discontinuous Galerkin (RKDG) scheme is proposed in order to solve the system of ideal Magnetohydrodynamics (MHD) equations, as an extension to the previous results published in [7] which showed a discontinuous Galerkin scheme to the compressible Euler equations of gas dynamics. Some techniques used to control oscillations near discontinuities are also available in this work, for example the limiting procedure used in [7] and the shock indicator criteria introduced in [6, 10]. In order to ensure the divergence free condition on the magnetic field, the Godunov symmetrization procedure is followed [2], modifying the MHD system by adding the so-called Powell terms [12]. Two different numerical fluxes are used in

Juan Pablo Gallego-Valencia
University of Würzburg, Campus Hubland Nord Emil-Fischer-Strae 40 97074 Würzburg Germany, e-mail: juan.gallego@mathematik.uni-wuerzburg.de

Christian Klingenberg
University of Würzburg, Campus Hubland Nord Emil-Fischer-Strae 40 97074 Würzburg Germany, e-mail: christian.klingenberg@mathematik.uni-wuerzburg.de

Praveen Chandrashekar
Tata Institute for Fundamental Research, Sharada Nagar, Chikkabommsandra Bangalore 560065 Karnataka, India, e-mail: praveen@tifrbng.res.in

the DG scheme, a local Lax-Friedrichs flux and an entropy stable flux introduced in [4]. Numerical test cases are presented to show the performance of the scheme through convergence rates and a direct comparison to the Athena Code [8].

2 Ideal MHD equations

The ideal magneto-hydrodynamical model, or ideal MHD equations, is a system of equations which describes the conservation of mass, momentum, energy, and magnetic field of a particular fluid. This system can be written in two dimensions as the conservation law system

$$\mathbf{q}_t + \nabla_{\mathbf{x}} \cdot \mathbf{F}(\mathbf{q}) = 0, \tag{1}$$

with

$$\mathbf{q} = [\rho, \mathbf{m}, \mathbf{B}, e]^T, \;\; \mathbf{F}(\mathbf{q}) = [\mathbf{f}_1(\mathbf{q}), \mathbf{f}_2(\mathbf{q})], \tag{2}$$

$$\mathbf{f}_1 = \begin{bmatrix} m_1 \\ \frac{m_1^2}{\rho} + p - B_1^2 \\ \frac{m_1 m_2}{\rho} - B_1 B_2 \\ \frac{m_1 m_3}{\rho} - B_1 B_3 \\ 0 \\ \frac{m_1}{\rho} B_2 - B_1 \frac{m_2}{\rho} \\ \frac{m_1}{\rho} B_3 - B_1 \frac{m_3}{\rho} \\ \frac{m_1}{\rho}(E+p) - \frac{B_1}{\rho}(\mathbf{m}\cdot\mathbf{B}) \end{bmatrix} \quad \mathbf{f}_2 = \begin{bmatrix} m_2 \\ \frac{m_2 m_1}{\rho} - B_2 B_1 \\ \frac{m_2^2}{\rho} + p - B_2^2 \\ \frac{m_2 m_3}{\rho} - B_2 B_3 \\ \frac{m_2}{\rho} B_1 - B_2 \frac{m_1}{\rho} \\ 0 \\ \frac{m_2}{\rho} B_3 - B_2 \frac{m_3}{\rho} \\ \frac{m_2}{\rho}(E+p) - \frac{B_2}{\rho}(\mathbf{m}\cdot\mathbf{B}). \end{bmatrix} \tag{3}$$

where ρ is the density, $\mathbf{m} = [m_1, m_2, m_3]^T$ is the momentum vector, p is the pressure, E is the total energy and $\mathbf{B} = [B_1, B_2, B_3]^T$ is the vector of magnetic components in each space dimension.

Since an additional relation is needed to close the system, the following equation of state is used, where the total energy is a function of the thermal pressure, the kinetic energy and the magnetic pressure

$$E = \frac{p}{\gamma - 1} + \frac{1}{2\rho}|\mathbf{m}|^2 + \frac{1}{2}|\mathbf{B}|^2.$$

Here γ is the adiabatic constant dependent on the type of gas. Finally, the magnetic field of this system of equations should satisfy the divergence free condition

$$\nabla \cdot \mathbf{B} = 0, \tag{4}$$

By calculating the Jacobian matrices $\mathbf{A}_1$ and $\mathbf{A}_2$ from $\mathbf{f}_1$ and $\mathbf{f}_2$ respectively, one realizes that they are singular, which means that the system is weakly hyperbolic. The set of eigenvalues for a Jacobiam matrix $\mathbf{A}_\kappa$, are found to be

- a zero eigenvalue $\lambda_0 = 0$,
- one entropy wave with speed $\lambda_e = u_\kappa$,
- two Alfvèn waves with speeds $\lambda_a^{\pm} = u_\kappa \pm \frac{B_\kappa}{\sqrt{\rho}}$, and
- four magneto acoustic waves with speeds $\lambda_{f,s}^{\pm} = u_\kappa \pm c_{f,s}$,

where $\mathbf{u} = [u_1, u_2, u_3]^T$ is the vector of speeds which can be calculated by dividing each momentum component m_κ by the density ρ. Finally c_f and c_s stand for the fast and slow speeds given by

$$c_{f,s}^2 = \frac{1}{2}\left(a^2 + b^2\right) \pm \frac{1}{2}\sqrt{(a^2+b^2)^2 - 4a^2(b\cdot\mathbf{n})^2}.$$

Here $a = \sqrt{\frac{\gamma p}{\rho}}$ is the sound speed in the fluid and $b := \frac{1}{\sqrt{\rho}}\mathbf{B}$, which means that $b^2 = \frac{1}{\rho}|\mathbf{B}|^2$ and $\mathbf{n}$ is a normal vector.

Divergence free condition $\nabla\cdot\mathbf{B} = 0$

In order to deal with the divergence free condition, a method based on the Godunov symmetrization of the MHD system shown in [2] will be used. This method arrives to the same modified system of equations published by Powell [12].

It modifies the eigensystem in primitive variables by replacing the zero eigenvalue (the κth-magnetic component) in each of the Jacobian matrices $\mathbf{A}_\kappa$ by a second advection wave with speed $\lambda = u_\kappa$. The system becomes hyperbolic and the Jacobian matrices are no longer singular. This is done by adding the following source term $\varphi'(\mathbf{q})\nabla\cdot\mathbf{B}$ to the conservation form of the MHD equations as follows

$$\partial_t \mathbf{q} + \nabla_x\cdot\mathbf{F}(\mathbf{q}) + \varphi'(\mathbf{q})\nabla_x\cdot\mathbf{B} = 0, \tag{5}$$

where $\varphi'(\mathbf{q}_h) = [0, \mathbf{B}, \mathbf{u}, \mathbf{u}\cdot\mathbf{B}]^T$. The resulting system is non-conservative, but the additional terms are multiples of $\nabla\cdot\mathbf{B}$, so when its initial condition is zero it will be zero for any time for the exact solution of the PDE. Numerically it is expected that these terms should remain very small, at least for smooth solutions.

3 Discontinuous Galerkin semi-discrete scheme for the MHD system

The domain Ω is discretized by a tessellation T over the set $\overline{\Omega}$. The tessellation used here is a Cartesian grid with the following characteristics

- $\overline{\Omega} = \bigcup_{\ell=1}^{N} \tau_\ell$,
- each $\tau \in T$ is a closed set and the interior of τ^{o} is non-empty,
- $\tau_i^{\mathrm{o}} \cap \tau_j^{\mathrm{o}} = \varnothing$, $\forall i \neq j, \tau_i, \tau_j \in T$.

As a result, and assuming that $\mathbf{q}_\ell$ is the solution of the initial value problem (IVP)

$$\begin{cases} \partial_t \mathbf{q} + \nabla_{\mathbf{x}} \cdot \mathbf{F}(\mathbf{q}) + \varphi'(\mathbf{q}) \nabla_x \cdot \mathbf{B} = 0, \\ \mathbf{q}(0,\mathbf{x}) = \mathbf{q}_0(\mathbf{x}), \end{cases} \tag{6}$$

in the cell $\tau_\ell \subset \Omega$, the solution $\mathbf{q}(t,\mathbf{x})$ to the PDE in the whole domain Ω can be written as the sum of the local solutions from each cell τ_ℓ of the tessellation T. That is

$$\mathbf{q}(t,\mathbf{x}) = \sum_{\ell=0}^{N} \mathbf{q}_\ell(t,\mathbf{x}) \chi_\ell(\mathbf{x}), \text{ where } \chi_\ell(\mathbf{x}) = \begin{cases} 1 & \text{if } \mathbf{x} \in \tau_\ell \\ 0 & \text{otherwise} \end{cases}$$

Let $\mathscr{V}_h^k$ be a test function space, defined as

$$\mathscr{V}_h^k = \{\phi \in L^p(D) : \phi|_{\tau_\ell} \in \mathbb{Q}^k(\tau_\ell),\ \forall \ell = 1,...,N\},$$

where $\mathbb{Q}^k(\tau_\ell)$ is the space of tensor product Legendre polynomials of degree k in the cell τ_ℓ. By writing the approximated solution $\mathbf{q}_h$ as a linear combination of functions $\phi(x,y) \in \mathscr{V}_h^k$.

$$\mathbf{q}_h = \sum_{j=1}^{(k+1)^2} \tilde{\mathbf{q}}_j(t) \phi^{(j)}(x,y).$$

Then in order to solve the IVP in equation (6), the following discontinuous Galerkin (DG) semi-discrete scheme is proposed $\forall \tau_\ell \in T$

$$\int_{\tau_\ell} \left[\partial_t \mathbf{q}_h v_h - \nabla v_h \cdot (\mathbf{f}(\mathbf{q}_h) + \mathbf{g}(\mathbf{q}_h)) + v_h \varphi'(\mathbf{q}_h) \nabla \cdot \mathbf{B}\right] d\mathbf{x} \\ \int_{\partial \tau_\ell} \left[\mathscr{H}\left(\mathbf{q}_h^-, \mathbf{q}_h^+, \mathbf{n}\right) + \frac{1}{2} \varphi'\left(\mathbf{q}_h^-\right) \left(\mathbf{B}^+ - \mathbf{B}^-\right) \cdot \mathbf{n}\right] v_h^- d\sigma = 0, \tag{7}$$

where $\mathscr{H}\left(\mathbf{q}_h^-, \mathbf{q}_h^+, \mathbf{n}\right)$ is a consistent numerical flux, $\mathbf{n}$ is a vector normal to the interface in $\partial \tau_\ell$ where the numerical flux is computed, $\mathbf{q}^-$ and $\mathbf{q}^+$ are respectively the values of $\mathbf{q}_h$ from the inside and outside of the cell τ_ℓ at each interface $\partial \tau_\ell$.

Two different numerical fluxes were used in this work, the first one is a local Lax-Friedrichs-type (LXF) numerical flux of the form.

$$\mathscr{H}(\mathbf{q}^+, \mathbf{q}-, \mathbf{n}) = \frac{1}{2}\left(\mathbf{F}(\mathbf{q}^+) + \mathbf{F}(\mathbf{q}^-)\right) - \frac{\lambda_{max,\tau_\ell}}{2}\left(\mathbf{q}^+ - \mathbf{q}^-\right) \tag{8}$$

where λ_{max,τ_ℓ} is the maximum eigenvalue of the Jacobian matrix of system at the cell τ_ℓ. The second numerical flux used was introduced in [4] and it was initially designed for a Finite Volume entropy stable scheme, and its general form is given by

$$\mathscr{H}(\mathbf{q}^-, \mathbf{q}^+, \mathbf{n}) = \mathscr{H}^*(\mathbf{q}^-, \mathbf{q}^+, \mathbf{n}) - \frac{1}{2} D(\mathbf{q}^-, \mathbf{q}^+)(\mathbf{q}^+ - \mathbf{q}^-), \quad D = D^T \geq 0 \tag{9}$$

where $\mathscr{H}^*(\mathbf{q}^-,\mathbf{q}^+,\mathbf{n})$ components are defined as

$$
\begin{aligned}
\mathscr{H}_1^* &= \hat{\rho}\overline{u}_n \\
\mathscr{H}_2^* &= P^* n_1 + \overline{u}_1\mathscr{H}_1^* - \overline{B}_n\overline{B}_1, \quad P^* = \frac{\overline{\rho}}{2\overline{\beta}} + \frac{1}{2}|\mathbf{B}|^2 \\
\mathscr{H}_3^* &= P^* n_2 + \overline{u}_1\mathscr{H}_1^* - \overline{B}_n\overline{B}_2, \\
\mathscr{H}_4^* &= P^* n_3 + \overline{u}_1\mathscr{H}_1^* - \overline{B}_n\overline{B}_3, \\
\mathscr{H}_5^* &= \frac{1}{\overline{\beta}}\left(\overline{\beta u_n}\overline{B}_1 - \overline{\beta u_1}\overline{B}_n\right) \\
\mathscr{H}_6^* &= \frac{1}{\overline{\beta}}\left(\overline{\beta u_n}\overline{B}_2 - \overline{\beta u_2}\overline{B}_n\right) \\
\mathscr{H}_7^* &= \frac{1}{\overline{\beta}}\left(\overline{\beta u_n}\overline{B}_3 - \overline{\beta u_3}\overline{B}_n\right) \\
\mathscr{H}_8^* &= \frac{1}{2}\left[\frac{1}{(\gamma-1)\hat{\beta}} - \overline{|\mathbf{u}|^2}\right]\mathscr{H}_1^* + \overline{u_1}\mathscr{H}_2^* + \overline{u_2}\mathscr{H}_3^* + \overline{u_3}\mathscr{H}_4^* \\
&\quad + \overline{B_1}\mathscr{H}_5^* + \overline{B_2}\mathscr{H}_6^* + \overline{B_3}\mathscr{H}_7^* - \frac{1}{2}\overline{u_n}\overline{|\mathbf{B}|^2} + \left(\overline{u_1}\overline{B_1} + \overline{u_2}\overline{B_2} + \overline{u_3}\overline{B_3}\right)\overline{B_n}
\end{aligned}
$$

Here $u_n = \mathbf{u}\cdot\mathbf{n}$ and $B_n = \mathbf{B}\cdot\mathbf{n}$ denote the normal component of the vectors $\mathbf{u}$ and $\mathbf{B}$ to the interface for which the numerical flux is being computed, the values n_i are the components of the normal vector $\mathbf{n}$, the operator $\overline{(\cdot)}$ denotes the arithmetic average between the values at both sides of the interface and the operator $\hat{(\cdot)}$ denotes the logarithmic average denoted respectively by

$$\overline{\eta} = \frac{1}{2}(\eta^- + \eta^+), \quad \hat{\eta} = \frac{\eta^+ - \eta^-}{\ln(\eta^+) - \ln(\eta^-)}.$$

The dissipation matrix D in (9) is a semi-definite positive matrix similar to the dissipation used in a Roe-type scheme. It is calculated using the scaled right eigenvectors matrix $\tilde{R}$ of symmetrization procedure to transform from conserved to entropy variables shown in [2, 4], as follows

$$D = \tilde{R}\Lambda\tilde{R}^{-1} \tag{10}$$

These quantities were introduced by Chandrashekar and Klingenberg to ensure the entropy stability of the Finite Volume scheme presented in [4].

This work will investigate the results using an explicit strong stability preserving (SSP) third order Runge-Kutta (RK) time integration (as the one used in [5] and [7]) when it is applied to an entropy stable scheme designed at the semi-discrete level.

Limiting procedure

For discontinuous solutions, it is necessary to use some limiting procedure to ensure non-oscillatory solutions. TVD-type limiters have been implemented inside the code.

It has been pointed out in [7] the advantage in limiting over the characteristic variables instead of the conserved variables. It is basically a procedure in which the Jacobian matrices are diagonalized, then the limiting procedure is applied over the characteristic variables of the system and finally the system is transformed back to the conserved variables.

The diagonalization procedure used in this work, was introduced by Bristo and Wu in [3], and it was also used in [9]. With other eigensystems, it may happen that the eigenvectors develope singularities in points where the eigenvalues degenerate. On the other hand, the eigensystem introduced in [3] has a proper choice of normalization, which avoids singularities in the eigenvectors and guarantees a complete set of eigenvectors.

Additional to the limiting procedures implemented in the code, a shock indicator introduced in [6] and [10] was also implemented and used in order to detect the places where the limiting procedure has to applied.

This shock indicator is based on the fact that for smooth regions the DG solution shows super-convergent approximation at the outflow boundaries of the cells. As the super-convergence is lost one can determine that the cell contains a discontinuous solution. The indicator criteria is defined as

$$\frac{|\int_{\partial\tau_\ell^-}(r_h^- - r_h^+)d\sigma|}{h^{\frac{k+1}{2}}|\partial\tau_\ell^-|\|r_h\|_{\tau_\ell}} > 1, \tag{11}$$

were r is either a determined variable (for example the density or the energy) or a function of them (like the entropy), $\partial\tau_\ell^-$ represent the set of outflow interfaces of the element and h is a characteristic length of the element.

4 Numerical implementation

The results presented in this work are an extension of the work in [7], which simulations were performed with the `dflo` code. The `dflo` code is an application based in the `deal.II` C++ libraries [1], and was initially developed to solve the compressible Euler equations of gas dynamics, and now it can solve the MHD equations with the following characteristics

- works on a Cartesian grid,
- uses explicit time integration with third order accuracy (SSP Shu scheme),
- uses tensor product Legendre polynomial basis,
- can use average gradient limiter (on the characteristic or the conserved variables), described in [7],

- can use the KXRCF shock indicator based on super-convergence, introduced in [6] and [10],
- for the MHD equations, either a local Lax-Friedrichs (LXF) or an entropy stable (ES) numerical flux described in [4] can be used.

4.1 Polarized Alfvèn wave test-case

The first MHD test case presented in this work is the Polarized Alfvèn wave, which is described by Tóth in [13], however the setup of the implementation was taken from [8] with a different orientation.

On a rectangular domain $\left[0, \frac{\sqrt{5}}{2}\right] \times \left[0, \sqrt{5}\right]$, a grid of $n \times 2n$ square cells is used with periodic boundary conditions. The Alfvèn wave is fixed to propagate in the direction $\tan^{-1}(\frac{1}{2}) \approx 26.6^o$ with respect to the x axis. The density and pressure are constants fixed to $\rho = 1$ and $p = 0.1$.

Then the values of the magnetic field are given by $B_{\parallel} = 1$, $B_{\perp} = 0.1\sin(2\pi x_{\parallel})$ and $B_3 = 0.1\cos(x_{\parallel})$ and the velocities are given by $u_{\parallel} = 0.1$, $u_{\perp} = 0.1\sin(2\pi x_{\parallel})$ and $u_3 = 0.1\cos(2\pi x_{\perp})$. In Cartesian coordinates the expressions for the velocity components are

$$u_1 = u_{\parallel}\cos(\theta) - u_{\perp}\sin(\theta), \;\; u_2 = u_{\parallel}\sin(\theta) + u_{\perp}\cos(\theta), \;\; u_3 = 0.1\cos(\theta_0) \quad (12)$$

and for the magnetic field components are

$$B_1 = B_{\parallel}\cos(\theta) - B_{\perp}\sin(\theta), \;\; B_2 = B_{\parallel}\sin(\theta) + B_{\perp}\cos(\theta), \;\; B_3 = 0.1\cos(\theta_0) \quad (13)$$

where $\theta = \tan^{-1}(\frac{1}{2})$ and $\theta_0 = 2\pi(x_1\cos(\theta) + x_2\sin(\theta))$. Due to the periodicity of the test case, the solution will return to the initial state every $\Delta t = 1.0$.

This test case was simulated with two different numerical fluxes, and four different grid sizes. Since the solution is smooth and periodic, convergence rates where computed for $t = 5$ (Table 1). It can be seen that for $\mathbb{Q}^1$ polynomial basis the results are very similar for both numerical fluxes, however for $\mathbb{Q}^2$ the errors produced by the ES numerical flux are considerably smaller than those from the LXF flux for both time levels.

Finally, Table 2 shows the L^{∞}-errors and convergence rates for the $\nabla \cdot \mathbf{B} = 0$ condition at $t = 5.0$. It can be seen that for $k = 1$ there are not significant differences between the use of the LXF flux and the ES flux. However, for $\mathbb{Q}^2$ the L^{∞}-errors are reduced considerably.

		LXF		ES	
	n	L^2-error	order	L^2-error	order
$\mathbb{Q}^1$	32	7.83E-04	–	9.30E-04	–
	64	1.60E-04	2.29	1.90E-04	2.29
	128	5.71E-05	2.10	4.47E-05	2.09
	256	7.59E-06	2.03	1.10E-05	2.02
$\mathbb{Q}^2$	32	1.58E-04	–	2.04E-05	–
	64	1.36E-05	3.54	1.49E-06	3.78
	128	9.56-07	3.83	1.56E-07	3.26
	256	6.66E-08	3.84	1.79E-08	3.12

Table 1 L^2- errors of the polarized Alfvèn test case at $t = 5.0$ using four different grid-sizes, $\mathbb{Q}^1$ and $\mathbb{Q}^2$ polynomial basis, and both the LXF and the ES numerical fluxes.

		LXF		ES	
	n	L^∞-error	order	L^∞-error	order
$\mathbb{Q}^1$	32	3.76E-02	–	5.12E-02	–
	64	1.88E-02	1.00	2.49E-02	1.04
	128	9.41E-03	1.00	1.23E-02	1.02
	256	4.71E-03	1.00	6.16E-03	1.00
$\mathbb{Q}^2$	32	1.72E-03	–	1.40E-03	–
	64	3.89E-04	2.14	3.95E-04	1.83
	128	1.83E-04	1.09	9.68E-05	2.03
	256	7.88E-05	1.22	2.41E-05	2.01

Table 2 L^∞-errors for the $\nabla \cdot \mathbf{B} = 0$ condition of the Polarized Alfvèn wave test case at $t = 5.0$, using $\mathbb{Q}^1$ and $\mathbb{Q}^2$ polynomial basis, the LXF and the ES flux, and four different grid-sizes.

4.2 Orszag-Tang vortex test-case

This test case was first introduced by Orszag and Tang in [11], and it has become a reference test case to validate numerical solutions for the MHD system. The set up of the test case is the following, in a square domain of $[0,1] \times [0,1]$ with periodic boundary conditions a gas ($\gamma = \frac{5}{3}$) has constant pressure $p = \frac{5}{12\pi}$ and density $\rho = \frac{25}{36\pi}$. The initial speeds are $u_1 = \sin(2\pi x_2)$ and $u_2 = \sin(2\pi x_1)$, and the initial values of the magnetic field are given by $B_1 = -B_0 \sin(2\pi x_2)$ and $B_2 = B_0 \sin(4\pi x_1)$, where $B_0 = \frac{1}{\sqrt{4\pi}}$.

The ES numerical flux was used for this test case, the limiting procedure used was the $\mathbb{Q}^k$ polynomial basis limiter introduced in [7], and also the KXRCF shock indicator will be activated only using the total energy (E) as indicator variable. The indicator is seen to be activated in regions of discontinuous solutions (Figure 1). The numerical solution is contrasted with the results of the Athena code in Figures 2 and 3, which shows good agreement between the two schemes.

The results using the ES numerical flux are quite close to the solution of the Athena code, but sometimes a bit more dissipative. The implementation presented here uses the Powell terms, which are known to add some dissipation to the scheme. An improvement can be done by using locally divergence-free basis, in which case the volume Powell terms are absent and this will reduce the dissipation.

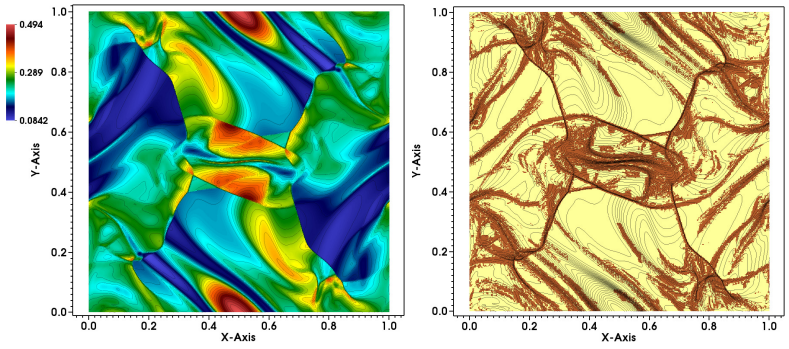

Fig. 1 (Left) Density values of the Orszag-Tang test case at $t = 0.5$. (Right) Trouble cells flagged by the shock indicator. ES numerical flux, $\mathbb{Q}^2$ polynomial basis, grid size $\Delta x_1 = \Delta x_2 = \frac{1}{512}$.

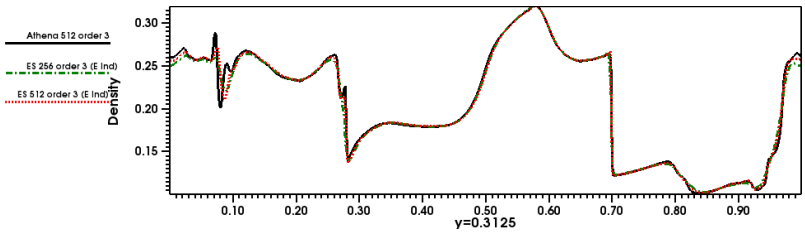

Fig. 2 Cut comparison ($y = 0.3125$) of the third order test case solution computed using the `dflo` code for two different grid sizes ($h = \{1/256, 1/512\}$) using the ES numerical flux, and the results from the Athena code for $h = 1/512$.

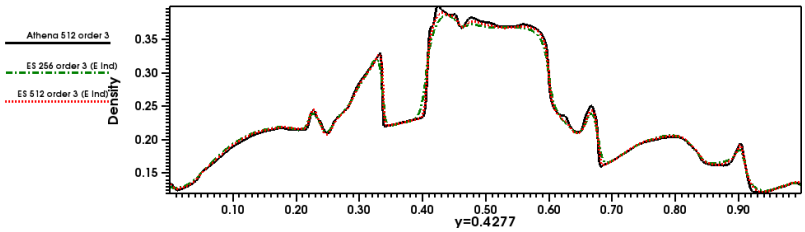

Fig. 3 Cut comparison ($y = 0.4277$) of the third order test case solution computed using the `dflo` code for two different grid sizes ($h = \{1/256, 1/512\}$) using the ES numerical flux, and the results from the Athena code for $h = 1/512$.

5 Conclusions

An explicit numerical scheme was proposed to solve the system of MHD equations. An entropy stable numerical flux designed initially for finite volumes was used in the context of DG. The numerical result show the expected order of approximation for smooth solutions and a performance comparable to well known methods as the Athena Code.

Acknowledgements JP G-V thanks the GRK 1147 and the DAAD STIBET fellowship at the University of Würzburg for their support.

References

1. Bangerth, W., Davydov, D., Heister, T., Heltai, L., Kanschat, G., Kronbichler, M., Maier, M., Turcksin, B., Wells, D.: The `deal.II` library, version 8.4. Journal of Numerical Mathematics **24** (2016)
2. Barth, T.J.: Numerical methods for gasdynamic systems on unstructured meshes. In: An introduction to recent developments in theory and numerics for conservation laws, pp. 195–285. Springer (1999)
3. Brio, M., Wu, C.C.: An upwind differencing scheme for the equations of ideal magnetohydrodynamics. Journal of computational physics **75**(2), 400–422 (1988)
4. Chandrashekar, P., Klingenberg, C.: Entropy stable finite volume scheme for ideal compressible mhd on 2-d cartesian meshes. SIAM Journal on Numerical Analysis (2016)
5. Cockburn, B., Shu, C.W.: The runge–kutta discontinuous galerkin method for conservation laws v: multidimensional systems. Journal of Computational Physics **141**(2), 199–224 (1998)
6. Flaherty, J.E., Krivodonova, L., Remacle, J.F., Shephard, M.S.: Aspects of discontinuous galerkin methods for hyperbolic conservation laws. Finite Elements in Analysis and Design **38**(10), 889–908 (2002). 2001 Robert J. Melosh Medal Competition
7. Gallego-Valencia, J.P., Klingenberg, C., Chandrashekar, P.: On limiting for higher order discontinuous galerkin method for 2d euler equations. Bulletin of the Brazilian Mathematical Society, New Series **47**(1), 335–345 (2016)
8. Gardiner, T.A., Stone, J.M.: An unsplit godunov method for ideal mhd via constrained transport. Journal of Computational Physics **205**(2), 509–539 (2005)
9. Jiang, G.S., Wu, C.c.: A high-order weno finite difference scheme for the equations of ideal magnetohydrodynamics. Journal of Computational Physics **150**(2), 561–594 (1999)
10. Krivodonova, L., Xin, J., Remacle, J.F., Chevaugeon, N., Flaherty, J.: Shock detection and limiting with discontinuous galerkin methods for hyperbolic conservation laws. Applied Numerical Mathematics **48**(3–4), 323–338 (2004). Workshop on Innovative Time Integrators for $\{$PDEs$\}$
11. Orszag, S.A., Tang, C.M.: Small-scale structure of two-dimensional magnetohydrodynamic turbulence. Journal of Fluid Mechanics **90**(01), 129–143 (1979)
12. Powell, K.G.: An approximate riemann solver for magnetohydrodynamics (that works in more than one dimension). Tech. rep. (1994)
13. Tóth, G.: The $\nabla \cdot b = 0$ constraint in shock-capturing magnetohydrodynamics codes. Journal of Computational Physics **161**(2), 605–652 (2000)